Etched Mirror and Groove-Coupled GaInAsP/InP Laser Devices for Integrated Optics

LARRY A. COLDREN, FELLOW, IEEE, KAZUHITO FURUYA, MEMBER, IEEE, BARRY I. MILLER, AND JOHN A. RENTSCHLER

Abstract—Recent advances in wet and dry etching techniques for GaInAsP/InP laser structures allow the reproducible fabrication of planar and vertical walled facets and grooves. These elements provide efficient mirrors and interstage couplers that may provide the basis for a new generation of monolithic integrated optical devices. Initial experimental results on etched facet lasers and groove-coupled two-section lasers verify theoretical expectations.

I. Introduction

RECENT advances [1]-[4] in wet and dry etching techniques for GaInAsP/InP structures may provide the basis for a new generation of integrated optical devices in these materials. These new techniques employ highly anisotropic reactive ion etching [1]-[3] and wet chemical etching, combined with crystallographic wet etches [4], [5] that effectively stop at certain desired crystal planes. For the first time it is conceivable that a practical chemical etching process may replace the cleaving step in the formation of mirrors for injection lasers. Of course, once the necessity for cleaving is eliminated, the laser substrate can take on arbitrary dimensions and the door is opened for the monolithic integration of other compatible and complementary devices with the laser. Moreover, the ability to etch a narrow groove with these new etching techniques provides a means to efficiently optically couple two adjacent integrated devices while maintaining electrical isolation [6].

The desire to form laser mirror facets by chemical etching is certainly not new. In fact, many reports of important advances in this field have appeared [7]-[12] and many of these have discussed and given initial evidence of the promising capabilities of etched facet devices. However, the questionable facet quality and reproducibility of most prior etching techniques have generally discouraged any practical implementation thereof. Also, there has been some work that illustrates the benefits of optically coupling together two device sections on a single chip [13]-[15]. Here again because of the marginal technology, practicality has been a question, although longitudinal mode control has been demonstrated.

In this paper, we provide evidence to show that etched facet and groove devices fabricated with the new etching procedures perform at near ideal levels. First, the etching procedures are summarized. Techniques to form either $(01\bar{1})$ or (011) plane facets as well as $(01\bar{1})$ bounded grooves are reviewed. Then, results from simple etched facet and short cavity configurations are given. In the fourth section, the characteristics of groove-coupled multisection lasers are studied. And, in the final section, we attempt to summarize these results and put them into perspective.

Manuscript received March 2, 1982; revised May 19, 1982.

L. A. Coldren, B. I. Miller, and J. A. Rentschler are with Bell Laboratories, Holmdel, NJ 07733.

K. Furuya was with Bell Laboratories, Holmdel, NJ 07733. He is now with the Department of Physical Electronics, Tokyo Institute of Technology, Tokyo, Japan.

II. Etched Facet Technology

Fig. 1 gives examples of several etching techniques we have explored. The first, which we have labeled WCE, is taken from Iga *et al.* [7] and it represents some of the best work done with standard wet chemical etching (WCE) to form laser facets. Most of the literature describes work using this general kind of technique [7]-[12]. In WCE, it is desirable to use an etchant that 1) etches both the cladding and active layers of the GaInAsP/InP laser at nearly the same rate, 2) provides a nearly vertical and smooth wall profile, and 3) results in little or no mask undercut. Unfortunately, no single etch has been found to do all this, although occasionally some have come close. The main problem with WCE is poor reproducibility. Wall slopes are generally curved, and masks are usually significantly undercut. Also, only mask edges that lie in the $(01\bar{1})$ plane on (100) substrates result in facets which approach vertical. For the orthogonal (011) orientation, the $(111)A$ plane prevents etching beyond a 55° outwardly sloping wall (positive slope).

The second technique illustrated in Fig. 1 is reactive-ion-etching (RIE) [1]-[3]. This low pressure plasma etching process results in virtually no mask undercut, so it is particularly well suited for narrow grooves [5], [6]. Of course, it is necessary to use etch resistant metal masks. Also, the RIE wall profile is the same for all orientations, and no protrusion or recession of the different composition active layer is evident, as is often the case with WCE. The main problems produced by RIE of the III-V compounds are wall surfaces that are rough and striated and somewhat positively sloped [3]. Careful control of the etching process can reduce these effects, but reproducibility here is also a problem. We believe some of the problems stem from the marginal volatility of the In and Ga etch products in these cases. The RIE is usually performed with a $Cl_2 : O_2$ gas mixture in a 4:1 ratio near room temperature, although higher temperatures and a percentage of Ar gas is sometimes employed to aid in removing the interfering $InCl_x$ or $GaCl_x$ compounds [2], [3]. For Cl_2 based mixtures the pressure is usually ~2-4 mtorr. Substrate tilting, rocking, and translation have also aided in smoothing the RIE surfaces and controlling the wall slope. These techniques and others are the subject of continuing investigation.

Crystallographic wet chemical etching (XWCE) is defined as WCE with etchants that effectively stop at certain crystal

0018-9480/82/1000-1667$00.75

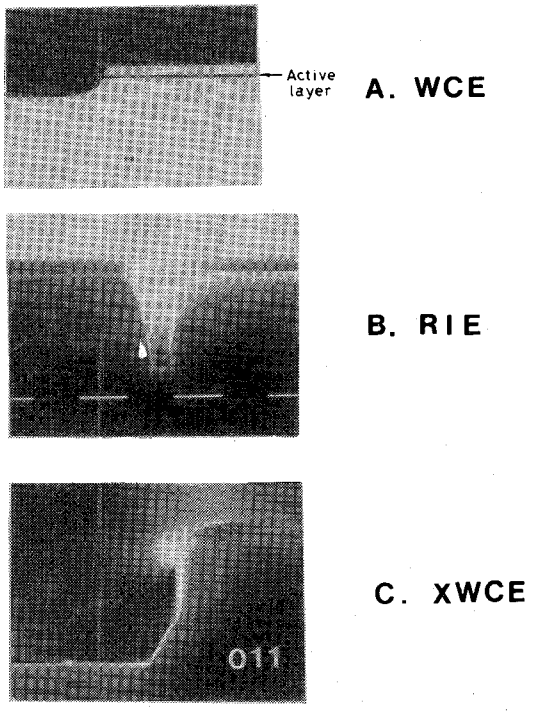

Fig. 1. SEM cross sections of etched facets using several etching techniques. WCE ≡ wet chemical etching after Iga *et al.* [7]. RIE ≡ reactive ion etching. XWCE ≡ crystallographic WCE. Marker bars = 1 μm, cross-sectional cleavage plane labeled.

planes, but have a significant etch rate slightly off this plane [4], [5], [16]. Thus, this plane tends to be exposed during etching. As shown in Fig. 1(c), very smooth, vertical, and planar facets are possible. The reproducibility in this case is very good.

Fig. 2 gives profile views of HCl and Br:methanol XWCE on two different orientations of InP. The sort of XWCE shown here and in Fig. 1(c) has been observed by many in the past, but no work has been published on its use for laser facets. One notable feature of the $(01\bar{1})$ wall created by HCl is the triangular protrusions hanging down from the mask edge. Below these "stalactite-like" protrusions that result from mask roughness, the surface is absolutely planar. The characteristic triangular shape is fortunate since it automatically eliminates the effect of mask roughness after some distance from the surface. Once the stop-etch plane is reached, very little undercutting occurs thereafter. How much undercutting occurs before it is reached appears to depend somewhat upon the masking material and how it was applied. Some mask-dependent variation in undercut has also been observed in etching to the $(111)A$ plane with Br:methanol [17], [18].

From the above we observe that HCl provides planar vertical $(01\bar{1})$ facets on (100) InP, and it is, thus, an obvious choice for laser mirrors. However, since HCl does not etch the quaternary active layer in the DH laser structure and no single chemical stop etches at the $(01\bar{1})$ on both InP and GaInAsP, we have developed a two-step procedure to form facets across a DH [4]. The first step uses either RIE or WCE to cut through all layers of the DH and provide an approximately vertical wall. The second step uses XWCE with HCl to planarize the facet. Fig. 3 gives a cross section and profile view of a laser facet etched in

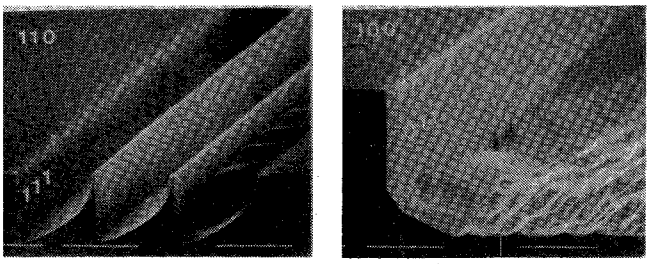

(a) (b)

Fig. 2. SEM profiles of etched facets on InP. (a) Triple grooves on (110) surface using 3 percent Br:methanol. $(111)A$ plane vertical with little undercut; $(111)B$ side is rounded with large undercut. (b) Single step on (100) surface using concentrated HCl. $(01\bar{1})$ plane exposed. Si_3N_4 masks; markers ≡ 10 μm.

this manner. Any slight protrusions and possible irregularities of the active layer can be lessened by a very brief material selective quaternary (Q) etchant either before or after the second step. A $K_3Fe(CN)_6$:KOH:H_2O mixture generally is employed [19]. If RIE is used in the first step, virtually no net undercut results following the HCl. This fact will be used later in our discussion of groove etching. For a WCE first step, we have found that a few HCl based mixtures still retain some stop-etch character, leading to the desired approximately vertical wall. However, we repeat that no true stop-etch mixtures have been found that etch both materials, and significant undercutting, as shown in Fig. 3, always occurs. Also, the mixtures generally leave an irregular surface. Mixtures of HCl:HNO_3 in 1:2-5 ratios, and HCl:CH_3COOH:H_2O_2 in 1:1-2:1 ratios have been studied.

By combining RIE with XWCE we can obtain some of the advantages of both, while avoiding some of their individual shortcomings. Two new device elements that have been derived from this marriage are the narrow plane-parallel groove [5] and the (011) planar facet [20]. The groove is useful in optically coupled two-section devices as will be discussed in Section IV. The (011) facet is very important for compatibility with state-of-the-art low-threshold lasers such as the buried heterostructure (BH) [21], [22], the buried crescent (BC) [23], or the crescent-shaped mesa substrate buried heterostructure (CMSB) [24], similar to the constructed double heterostructure (CDH) in AlGaAs [25]. These structures require crystal growth along a ridge or in a groove. In both cases of preferred laser axis is the [011]. Also, for the BH, the desirable "inverted V" occurs along the [011].

Fig. 4 illustrates the groove, and Fig. 5 shows an (011) facet on DH structures. As described in the figure caption the groove is formed by a sequence of RIE and XWCE steps with one intermediate quaternary etching step. The (011) facet is made possible by first using angled RIE [3] to cut slightly beyond a vertical angle, and then HCl to planarize the facet in a two-step procedure similar to that discussed above for $(01\bar{1})$ facets [20]. Note that here, since the $(111)A$ plane separates the (100) surface from the (011) vertical, WCE cannot provide the first step [16], [20]. All known wet etches are stopped by the $(111)A$ resulting in an outwardly sloping wall [26]. HCl has been shown to have essentially zero etch rate for wall slopes between 40 and 90° measured from the surface for this

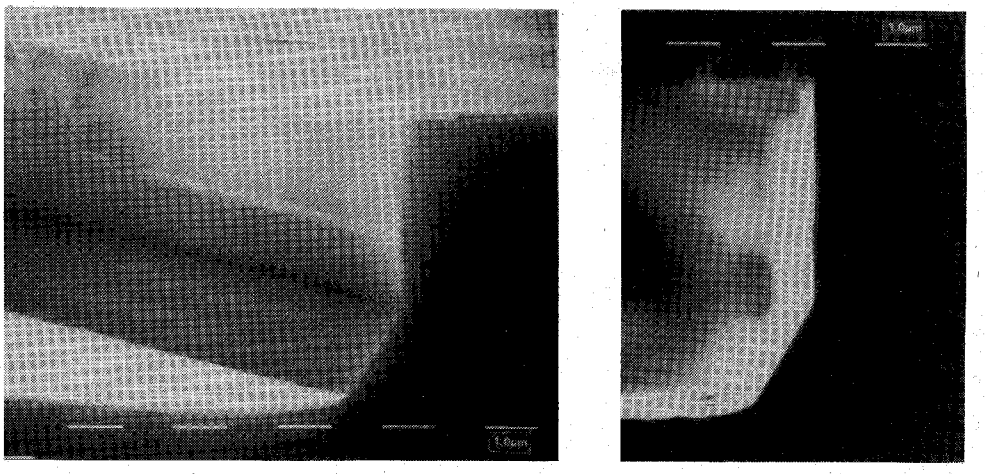

(a) (b)

Fig. 3. (a) SEM perspective and (b) cross-sectional view of the etched facet on DH wafer masked with Si_3N_4. The wafer was etched first with 1 HCl + 2HNO_3 for 20 s and then with concentrated HCl for 10 s.

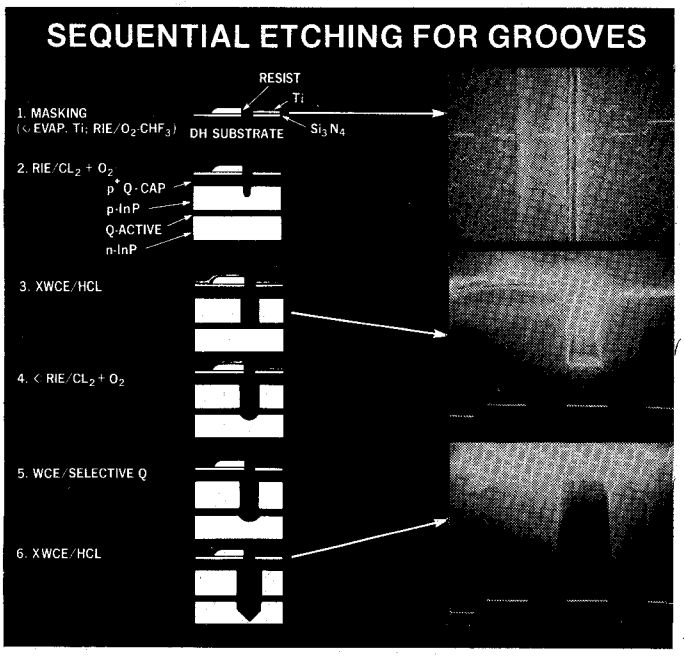

Fig. 4. Groove, etching sequence and illustrative SEM cross sections. 1) 2000 Å masking slot formed by angle evaporation of Ti over resist ridge, followed by RIE with O_2 and CHF_3 to remove resist residue and Si_3N_4. 2) RIE with 4:1, Cl_2:O_2 mixture @ 2 mtorr pressure and 0.3 W/cm^2 for 60 min. 3) Initial XWCE with HCl for 20 s to active. 4) Angled RIE @±5° for 10 min each. 5) $K_3Fe(CN)_6$: KOH:H_2O, 6:4:70 by wt for 10 s. 6) Final XWCE with HCl for 5 s. Marker ≡ 1 μm.

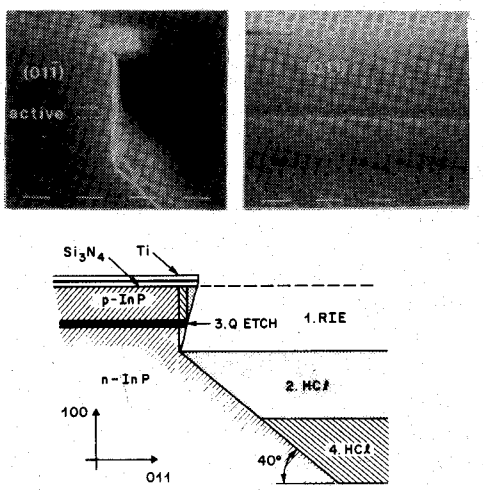

Fig. 5. (011) XWCE facet etching. (a) SEM cross section and perspective. (b) Sequence of steps in cross section. 1) Angled RIE @40° for 120 min. 2) HCl for 10 s. 3) $K_3Fe(CN)_6$ mixture for 10 s. 4) HCl for 10 s. Marker ≡ 1 μm.

masking orientation (i.e., mask edge located at the intersection of the (100) and (011) plane). Thus, the RIE must provide a wall slope a little beyond 90° so that the HCl will work [5], [16], [20]. In this case, the XWCE/HCl actually is masked at the bottom of the step where the wall slope becomes less than 90°. Thus, the characteristic protruding triangles come up from the bottom as can be seen in Fig. 5. Below where the RIE etched, the wall slopes at ~40°, as is normal for HCl on this orientation of InP [5], [16], [20], [26].

The characteristic protruding triangles mentioned above in reference to Figs. 2 and 5 have also been found to be useful in orientating (100) wafers prior to any photolithographic steps. By etching a small rectangle cleaved from a DH wafer or a nitride coated InP substrate in concentrated HCl for about 2 min, the characteristic triangular protrusions can be created on the cleaved edges [27]. If the triangular *protrusions* "hang-down" from the masked (100) surface, they lie on the (01$\bar{1}$) plane, conversely, if they point up, they lie on the (011) plane. Since the triangles are only formed by irregularities, it is important that the cleaves on the test piece be *imperfect*. Usually, a rather crudely scribed and broken sample is best.

III. Etched Facet Lasers

The crystallographic (XWCE) etching techniques outlined above have been used to fabricate a number of laser devices, the simplest of which is the broad area contact laser (entire DH laser chip pumped). These broad area lasers provide the best and most reliable data concerning the optical reflection properties of the etched facets, since their basic two-dimensional structure does not allow significant contributions

from electrical or optical loss mechanisms, as compared to their more sophisticated three-dimensional counterparts.

Fig. 6 gives the optical output power versus injection current for two sets of broad area devices taken from the same LPE wafer. The first set has one etched and one cleaved mirror, and the second has two cleaved mirrors for reference. The light is always collected from the cleaved end. Devices with bad I–V curves were not measured. Note that the two sets are qualitatively very similar. Since the etched-cleaved devices are somewhat wider, their thresholds are slightly higher. The differential quantum efficiencies are ~10–20 percent per facet for the etched-cleaved chips and ~15–20 percent per facet for the cleaved-etched devices.

Fig. 7 summarizes these data, as well as that from additional different length chips fabricated on the same wafer, by a plot of threshold versus reciprocal length. From this plot it is possible to estimate the etched facet reflectance R_E using the well-known relationship for threshold current density, of a laser of length l [8]

$$J_{th}(l) = J_{th}(\infty) + (A/l) \ln (r_1 r_2)^{-1} \quad (1)$$

where A is a constant and r_1 and r_2 are the reflectivities of the mirrors. The constants $J_{th}(\infty)$ and A are calculated from the cleaved data ($r_1 = r_2 = 0.556$) and the practical assumption that $J_{th}(\infty) \gtrsim 0.5$ kA/cm^2 (active Q-layer thickness ≈ 0.18 μm). The uncertainty in the calculated value for the etched facets $|r_1|^2 = R_E = (0.28 \pm 0.04)$, stems as much from the scatter in the cleaved data as from that in the etched-cleaved facet device data. Despite this uncertainty, it seems clear from both Figs. 6 and 7 that the etched facets do not provide a significant limitation on device performance.

Similar comparisons between cleaved and etched facet devices have also been carried out on gain-guided stripe geometry devices with similar results. However, we find that a quantitative estimate of facet quality is more elusive because of a greater spread in the data. For 10 μm wide stripes, no other current confining techniques, and a 250–300 μm length, we measure thresholds between 250 and 400 mA in both cases. Differential quantum efficiencies are also similar for cleaves and etched facets that look "good" under the SEM ("good" ≡ smooth with $\ll$1000 Å step or protrusion at the active layer).

Earlier results with facets formed by a single RIE step also gave reasonable threshold levels, although clearly somewhat higher than those of cleaved devices [1]. Not surprisingly, the more sensitive differential quantum efficiency showed a more significant departure from cleaved standards in the RIE case. The striated surface topology [1]–[3] is believed to be the cause. Since the RIE ions strike the etched wall at grazing incidence, no material damage is expected beyond the depth of the striations (~1000 Å). Also, good quantum efficiencies are observed after only a brief etching in HCl, which removes little material beyond the striations.

One obvious application of these new etching techniques is in the formation of short cavity lasers ($l \lesssim 50$ μm). Fig. 8 gives SEM profiles of a double etched facet short-cavity device. Since the devices were not mounted on heat sinks, and the

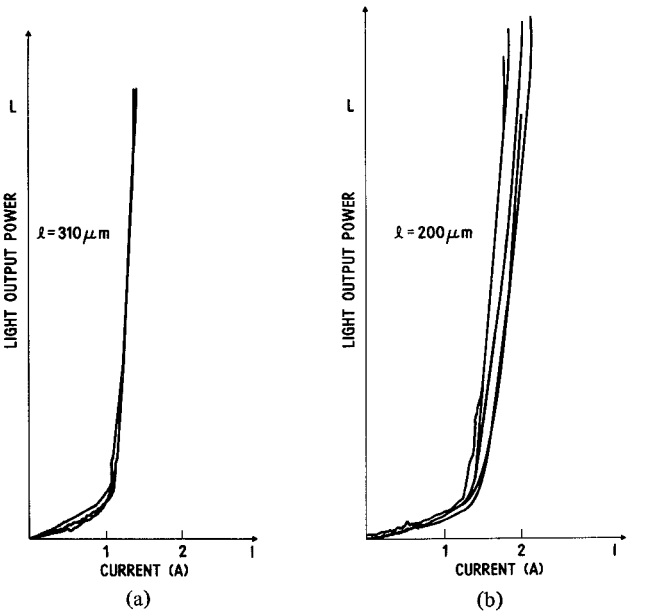

Fig. 6. Optical power out versus input current for broad area laser chips with (a) cleaved facets or (b) one cleaved and one etched facet.

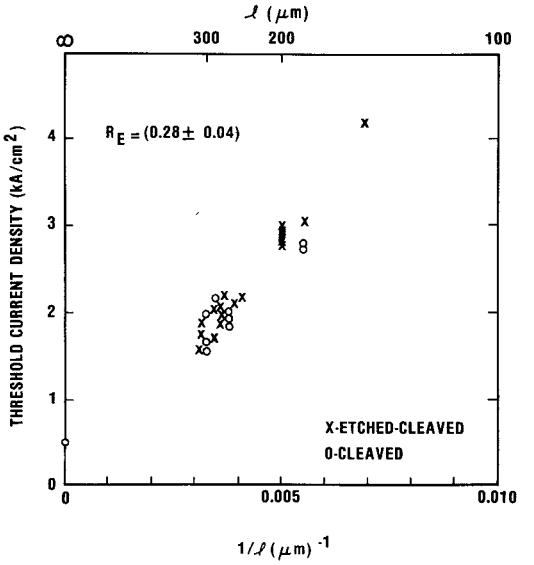

Fig. 7. Threshold current density versus reciprocal cavity length ($1/l$) for cleaved and etched facet lasers.

contact resistance was ~40 Ω, too much heating occurred at room temperature to reach lasing threshold even for 100 ns pulses. By cooling to ~10°C the devices did work as lasers. Similar work with short cleaved lasers [28], in which great care was taken to properly contact and heat sink the small chips, provided room-temperature operation as well as demonstrated the desired single longitudinal mode output. In our case, heat sinking and mounting should be easier since a relatively large substrate can remain attached. In gain-guided devices such as the above, single longitudinal mode is more difficult to obtain than in index guided structures [29], so we could expect even more consistent single longitudinal mode operation in a practical index-guided structure of this length.

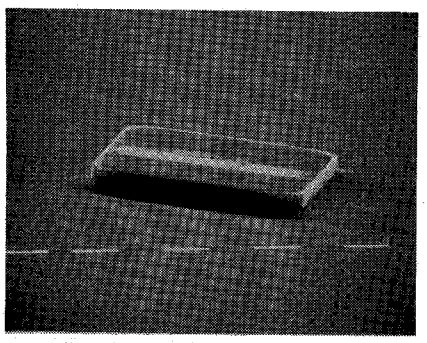

(a)

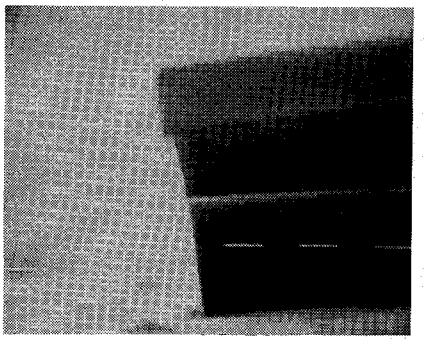

(b)

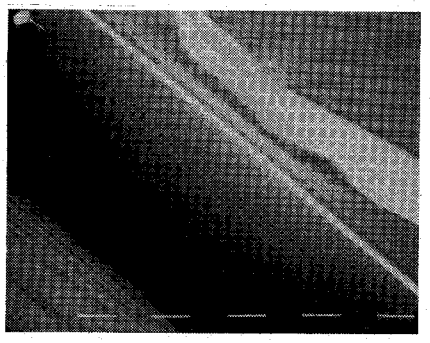

(c)

Fig. 8. Short cavity laser SEM views. (a) Overall, marker ≡ 10 μm; (b) facet cross section; and (c) facet perspective. Marker ≡ 1 μm.

IV. Groove-Coupled Two-Section Lasers

The benefits of coupling different length laser cavities together have been espoused by several authors [6], [13], [15], [30], [31]. Some of these same benefits, especially those resulting directly from the modified longitudinal mode structure of coupled cavities, can be obtained by using a short passive cavity coupled to a laser [13], [32]-[34]. A degree of mode filtering may also be possible by using a segmented injection electrode structure, even without any direct optical discontinuities. In what follows, we will concentrate on the particular characteristics of a monolithic two or more section laser device, optically interconnected either directly or through a narrow groove, and with separate electrical connections to each section.

The first demonstrations of these kinds of devices used a single RIE fabrication step to etch either a shallow or deep groove across a DH laser stripe [6]. The shallow grooves provided fair electrical isolation and weak optical discontinuity (or strong optical interstage coupling); the deep grooves gave good electrical isolation and strong optical discontinuity. As expected, current modulation in one cavity gave strong amplitude effects in the other for strong coupling (shallow) and strong spectrum effects for weak coupling (deep). Fig. 9 briefly reviews the spectrum effects for a deep RIE groove device (etching cuts across the active layer). Here, what we have termed the "active-etalon" effect [5], [6] is clearly evident. That is, the example illustrates a gain-guided stripe-geometry device with a long (1) and a short (2) cavity in which the bias to section 1, I_1, has been increased to the lasing threshold while $I_2 = 0$. All longitudinal modes of cavity 1 appear (lower curve). Then, the gain in the short etalon cavity is increased ($I_2 > 0$), selectively amplifying modes near its natural resonances (upper curve). In effect, one "mirror" of the long cavity has developed gain at a few select wavelengths while becoming even more lossy at all others. As much as 28 dB of intermediate mode suppression is observed in this example. The selected modes occur at l_1/l_2 times the original mode spacing consistent with etalon theory. The somewhat "dirty" quality of the spectra seems to be correlated with the use of the nonideal RIE mirrors. Use of the combined RIE-XWCE groove etching procedure provides much cleaner results as shown below.

One of the major anticipated advantages of using a two-section design is the provision of single longitudinal mode outputs even under high speed modulation. In previous monolithic devices, only with a high current density short-cavity design [7], [28] or a more complex distributed Bragg reflector [35] has there been any other real progress toward this goal. Of course the two-section is, in effect, a single-mode short cavity coupled to a longer one. The advantage over the short cavity alone is a much lower required current density and higher output powers. Moreover, the two-section approach has additional degrees of freedom afforded by the three-terminal geometry.

The present two-section devices have been operated in several different bias modes to provide single or quasi-single longitudinal mode operation under high speed modulation. Currents I_1 and I_2 can be modulated simultaneously, or one can be held on while the other is modulated. In this latter case the dc current can be either below or above the individual threshold of that cavity. Thus, many regimes of operation are possible. For example, if one cavity is lased continuously and the other is pulsed, the latter's output will tend to be "injection-locked" at a single common wavelength. Such injection locking has been widely studied using hybrid geometries [30], [36], [37].

Fig. 10 gives spectra from a device fabricated with a combined RIE-XWCE procedure in which the drive currents are either 200 or 1 ns duration pulses. As can be seen, the very same longitudinal modes appear with either near CW conditions (τ = 200 ns) or short pulse modulation (τ = 1 ns). Here, single longitudinal mode is not expected, since $l_1/l_2 \sim 5$. But, as expected, every fifth mode is enhanced by the active

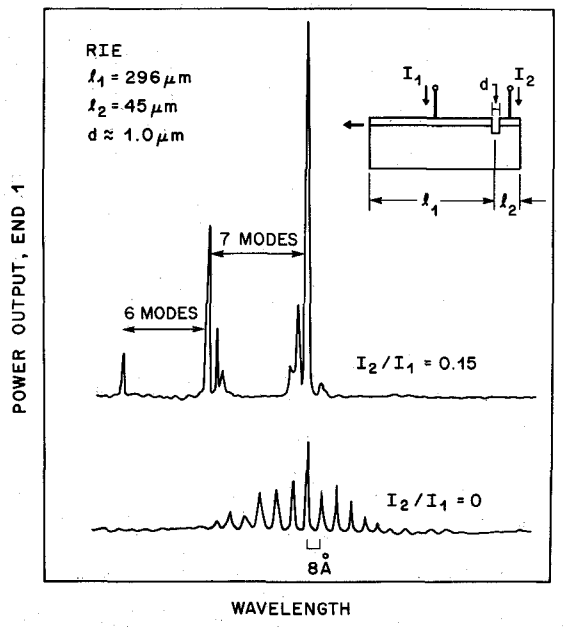

Fig. 9. Spectra from RIE two-section gain-guided stripe laser with a deep groove. Lower trace taken at threshold I_1 with $I_2 = 0$—all modes appear. Upper trace taken with same I_1 and significant gain in etalon section 2—only modes near cavity 2 resonance appear. Note that $l_1/l_2 \approx 6.6 \neq$ integer. Groove depth ≈ 4.1 μm. Contact stripe width ≈ 10 μm.

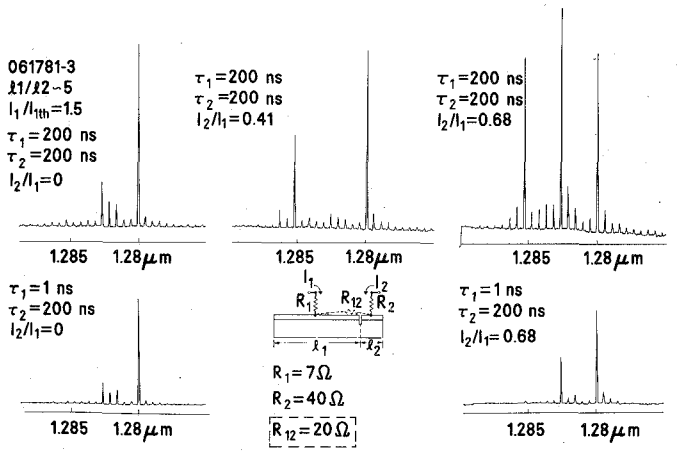

Fig. 10. Spectra from a XWCE-RIE two-section laser with either 200 ns or 1 ns current pulses. Measurements integrated over a ~20 ns gate in the center of the 200 ns pulses or encompassing the 1 ns pulses. Spectrometer resolution ≡ 0.1 Å for 200 ns and 0.5 Å for 1 ns drive. R_i's are net contact resistances. Groove depth ≈ 3.9 μm.

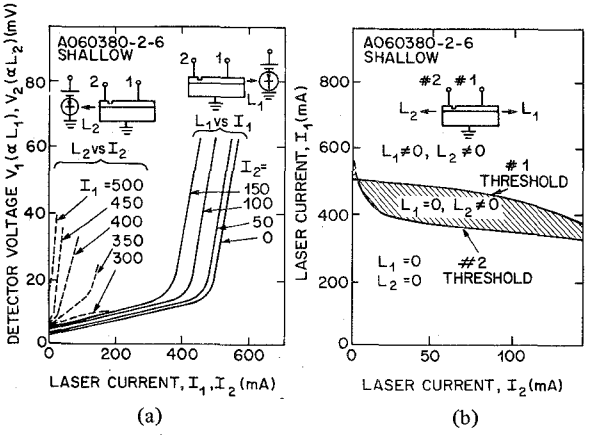

Fig. 11. Characteristics of a gain-guided shallow-groove two-section stripe laser. (a) Light output (∝ detector voltage) from each section (L_1 or L_2) versus its injection current (I_1 or I_2) with the other as a parameter. (b) Locus of threshold current conditions with regions labeled by lasing outputs L_1 and L_2. Groove depth ≈ 1.8 μm; active layer depth ≈ 2.2 μm; $l_1/l_2 \approx 8$.

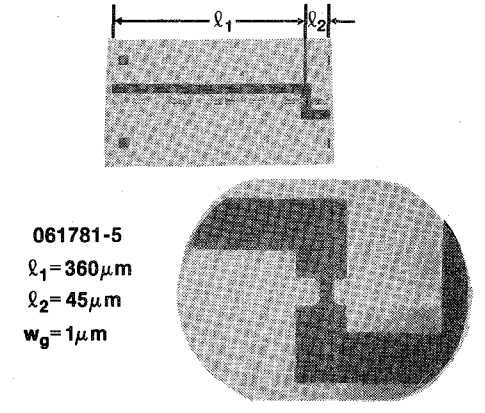

Fig. 12. Photomicrograph of the two-section device.

etalon. For these "worst case" gain-guided structures, $l_1/l_2 \gtrsim 10$ appears to be required for single mode with $l_1 \sim 300$ μm. With a more practical index guided laser structure, the requirement should be less stringent [29]. One notable defect in the device characterized in Fig. 10 is the poor electrical isolation between cavities, apparently caused by a Zn diffusion carried out after the groove was formed. This interconnection resistance R_{12} prevents us from individually controlling the two cavity currents to adjust the etalon finesse, as was demonstrated in Fig. 9. Thus, the intermediate modes are not greatly suppressed. However, we do observe a *cleaner* mode spectrum with the XWCE mirrors.

Fig. 11 summarizes the strong intercavity coupling effects inherent in a shallow groove device. In (a) the light out of one section is plotted as a function of the current applied to its contact as various fixed currents are injected in the other. The resulting families of curves illustrate the modulation which is possible by varying the gain in the other end [6]. Fig. 11(b) uses the same data to illustrate four regions of device operation, in which the light levels from each section are either below ($L_i \approx 0$) or above ($L_i \neq 0$) threshold.

We believe this type of three-terminal behavior may find a number of applications in future integrated optical circuits. For example, if the short section is used to modulate the long section, low current and higher speed may be possible. Also with this type of quasi-Q-switched operation the background light output due to spontaneous emission can be reduced. The spectral effects detailed above are also partially retained (depending upon the groove depth) so that we can also hope for single wavelength operation under fast modulation as suggested in Fig. 10.

The proper design and fabrication of the short cavity-long cavity type of device, as pictured in Fig. 12, as well as other groove-coupled devices, depend upon an understanding of the transmission and reflection properties of the grooves as well as the expected net cavity longitudinal mode spectrum resulting from the optical coupling. Wave scattering theory [38] gives an accurate and physically intuitive means of study-

ing and predicting these properties. For the groove we desire the net reflection S_{11} and the net transmission S_{12}. Assuming a plane-parallel groove of width d, a single facet reflectivity for the guided mode of $\pm r$, and amplitude transmission factors of t and t' (that account for diffraction and mode reexcitation loss for a single pass or roundtrip in the groove, respectively), we obtain the following:

$$S_{11} = r - \frac{rt'(1 - r^2)}{1 - r^2 t'} \tag{2}$$

$$S_{12} = \frac{t(1 - r^2)}{1 - r^2 t'}. \tag{3}$$

The transmission factors t and t', for propagation lengths d and $2d$, respectively, were calculated neglecting diffraction in the substrate plane (wide slab approximation) and using Gaussian diffraction perpendicular to the plane. These approximations lead to

$$t(d) = \sqrt{2w_o w(d)/[w^2(d) + w_o^2]}\; e^{-j\beta d} \tag{4}$$

where

$$t = t(d),\ t' = t(2d),\ w(d)^2 = w_o^2\,[1 + (\lambda d/\pi w_o^2)^2],$$

$\beta = 2\pi/\lambda$ is the propagation constant in the groove, and

$$w_o \approx 0.5h + 0.04\sqrt{\lambda/h} \tag{5}$$

is an effective Gaussian mode half-width for a quaternary active layer of thickness h cladded by InP. Fig. 12 plots the power reflection, transmission, and loss as a function of groove width for $h = 0.1$ μm at $\lambda = 1.3$ μm. Note that this $\lambda = 1.3$ μm result is approximately correct at 1.55 μm, if only the abscissa is scaled because of the weak λ dependence in (5). Subsequently, t and t' were also calculated exactly using the proper exponentially evanescent mode profiles and overlap integration [39] to yield nearly identical results, provided only the proper effective Gaussian width is used, as is the case in (4) and (5). Put another way, the empirical width w_o in (5) was obtained by fitting an assumed width of the form $Ah + B/h$ to the exact numerical results. It is a reasonable approximation for $0.08 < h < 0.3$ μm, $1.2 < \lambda < 1.6$ μm, and $0 < d < 2$ μm.

From the curves in Fig. 13 we observe that the net reflectance from a groove $|S_{11}|^2$ can be significantly larger than $|r|^2 = 0.31$, the single facet reflectance. Thus, for ideal grooves of the proper design, the threshold levels in both adjacent cavities can be reduced. This is true even while much of the transmitted energy is lost into radiation modes $(1 - |S_{11}|^2 - |S_{12}|^2)$ due to diffraction. This loss primarily reduces the intercavity coupling efficiency, a factor which is desirably small for spectrum control. On the other hand, for efficient amplitude modulation or other cases where efficient optical injection between the coupled cavities is important, good transmission is generally more important than reflection. An extremely narrow groove would fit the bill, but we have found, as shown in Fig. 11, that a shallow groove, which interacts only with the optical mode tails, provides the desired efficient transmission. The scattering loss in this case shows up primarily in the reflection efficiency.

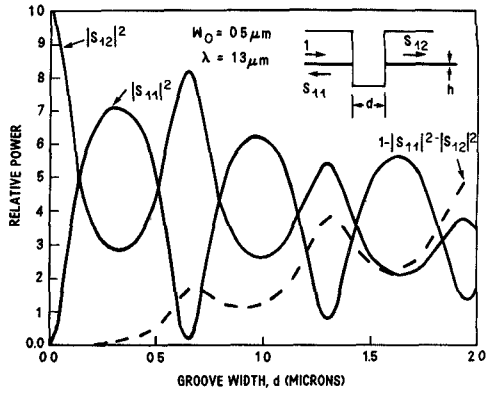

(a)

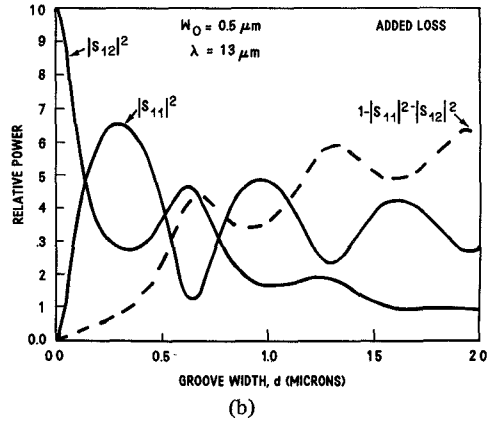

(b)

Fig. 13. Theoretical power transmission $|S_{12}|^2$, reflection $|S_{11}|^2$, and loss $(1 - |S_{11}|^2 - |S_{12}|^2)$ of grooves for a 1000 Å thick active layer of infinite width. (a) Plane-parallel walls using (4). (b) Loss added by arbitrarily decreasing transmission factor twofold from (4). Dashed line is the single facet reflectance.

The net mode structure of the two-section device was similarly calculated using a one-dimensional analysis. (That is, uniform waveguiding is assumed in the transverse directions.) Referring to the schematic in Fig. 14, we calculate the net transmission through the device assuming a small probe signal at one end. The net transfer function obtained from this linear analysis is then

$$H = \frac{t_1 t_2 S_{12}\sqrt{(1 - r_1^2)(1 - r_2^2)}}{1 + r_1 r_2 t_1^2 t_2^2 (S_{11}^2 - S_{12}^2) - S_{11}(r_1 t_1^2 + r_2 t_2^2)} \tag{6}$$

where $t_1 = e^{-jB_1 l_1}$ and $t_2 = e^{-jB_2 l_2}$ are the one-pass cavity transmission factors, in which the complex propagation constant $B_i = \beta_i - j\alpha_i$ includes the incremental propagation phase β_i and gain α_i constants. Equation (6) represents the net response of the coupled cavities below threshold optical power levels before saturation effects occur.

Two example length-combinations are considered in Fig. 14. In these plots the gains were increased until one mode develops a large net gain. In both cases the expected mode selection is evident; however, the $l_1 \gg l_2$ case provides the cleanest spectra. The advantage of the $l_1 \sim l_2$ geometry is that the current density (incremental gain) in each cavity is relatively low. As is always the case with short cavities, an increase in mirror reflectivity would help. As suggested above, the shallow groove case provides a large S_{12} and a small S_{11}. However,

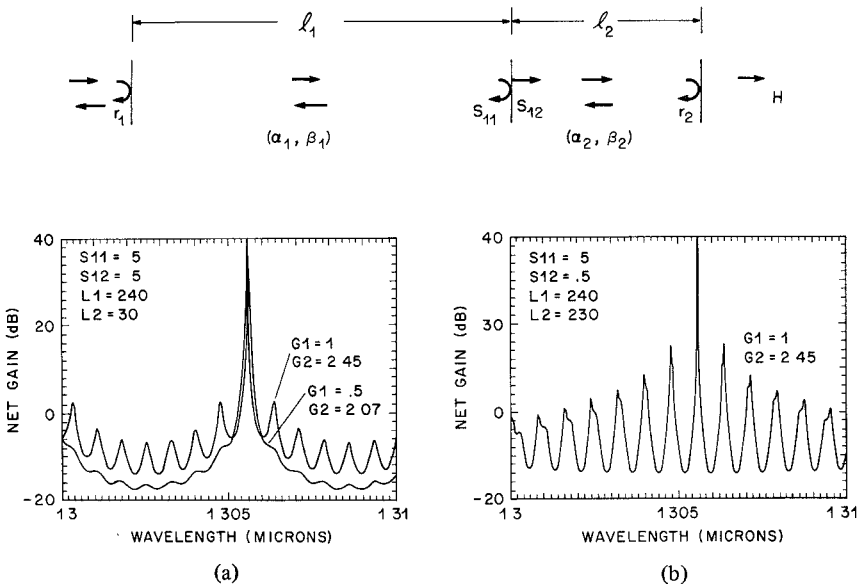

(a) (b)

Fig. 14. (a) Schematic representation of two-section laser for scattering theory. (b) Example response curves with $l_1 \gg l_2$ and $l_1 \sim l_2$. Net gain = $|H|^2$; $S11, S12 = S_{11}, S_{12}$; $G1, G2$ = net single pass gains = $e^{a_i l_i}$; $L1, L2 = l_1, l_2$.

even in this case (not shown) the net coupled-cavity transfer function can still show a sufficient spectrum modulation for longitudinal mode selection. Experiments have borne out these predictions. Thus, in cases where strong intercavity coupling is desired for amplitude effects, spectrum control is still possible, and a simple shallow groove may be sufficient.

V. Summary and Discussion

In the above, we have reviewed new etching techniques for laser mirrors and narrow coupling grooves, and we have provided evidence to illustrate the usefulness of these new and improved elements. Most significantly, we have shown that good lasers can be fabricated on relatively large area substrates, that either the $(01\bar{1})$ or the (011) plane can be used for mirrors, and that the longitudinal mode structure can be controlled, either with stand-alone short cavities or coupled two-section devices. The two-section devices can be designed to lase in one or a select few longitudinal modes. The output wavelength is held relatively constant as the drive current amplitude or pulse width is varied. Modulation with 1 ns pulses gives the same spectral lines as with 200 ns pulses. The three-terminal configuration permits a very desirable electronic control of the output properties.

The devices illustrated, and others only conceived, show promise for a number of applications. The obvious compatibility of the simple etched facet laser (short or long cavity) with complimentary electronics should permit progress in this area of integrated optics in the near future. Optical-to-optical device integration, either via a groove or an interconnecting butt-joined dielectric-waveguide [39] has already been demonstrated. High-speed, low-current modulation with reduced background levels and single wavelength emission is promised by the additional degrees of freedom in a two- or three-section laser device. For example, by use of optical injection from an adjacent section it is not necessary to electrically prebias the output stage for fast modulation, and its wavelength will tend to replicate that of the optical injection [30], [36], [37].

Acknowledgment

The authors would like to acknowledge C. A. Burrus, R. J. Martin, and L. W. Stulz for help and advice with contact formation, P. D. Wright for comments on the manuscript, and J. D. McGee for help in preparing and testing the DH wafers.

References

[1] L. A. Coldren, K. Iga, B. I. Miller, and J. A. Rentschler, "GaInAsP/InP stripe-geometry laser with a reactive-ion-etched facet," *Appl. Phys. Lett.*, vol. 37, pp. 681–683, 1980.

[2] R. E. Howard, E. L. Hu, and L. A. Coldren, "Reactive-ion-etching of III–V compounds," in *Proc. Top. Meet. Integrated and Guided Wave Opt.*, Incline Village, NV, 1980 (Opt. Soc. Amer.), paper WA-2.

[3] L. A. Coldren and J. A. Rentschler, "Directional reactive-ion-etching of InP with Cl_2 containing gases," *J. Vac. Sci. Technol.*, vol. 19, pp. 225–230, 1981.

[4] K. Furuya, L. A. Coldren, B. I. Miller, and J. A. Rentschler, "Crystallographic facets chemically etched in GaInAsP/InP for integrated optics," *Electron. Lett.*, vol. 17, pp. 582–583, 1981.

[5] —, "Etched mirrors, grooves, and surfaces for GaInAsP/InP integrated optical devices using stop-etch crystal planes," in *Proc. Top. Meet. Integrated and Guided Wave Opt.*, Pacific Grove, CA, 1982 (Opt. Soc. Amer.), paper WB-1.

[6] L. A. Coldren, B. I. Miller, K. Iga, and J. A. Rentschler, "Monolithic two-section GaInAsP/InP active-optical-resonator devices formed by reactive-ion-etching," *Appl. Phys. Lett.*, vol. vol. 38, pp. 315–317, Mar. 1981.

[7] K. Iga and B. I. Miller, "Chemically etched-mirror GaInAsP/InP lasers–Review," *IEEE J. Quantum Electron.*, vol. QE-18, pp. 22–29, Jan. 1982.

[8] J. L. Merz, R. A. Logan, and A. M. Sergent, "GaAs integrated optical circuits by wet chemical etching," *IEEE J. Quantum Electron.*, vol. QE-15, pp. 72–82, Feb. 1979.

[9] P. D. Wright, R. J. Nelson, and T. Cella, "InGaAsP double heterostructure lasers (λ = 1.3 μm) with etched reflectors," *Appl. Phys. Lett.*, vol. 36, pp. 518–520, Apr. 1980; also P. D. Wright, R. J. Nelson, and R. B. Wilson, "Monolithic integration of InGaAsP heterostructure lasers and electrooptical devices," *IEEE J. Quantum Electron.*, vol. QE-18, pp. 249–258, Feb. 1982.

[10] K. Iga, T. Kambayashi, K. Wakao, and C. Kitahara, "GaInAsP/InP DH lasers and related fabricating techniques for integration," *IEEE J. Quantum Electron.*, vol. QE-15, pp. 707–710, Aug. 1979.
[11] C. E. Hurwitz, J. A. Rossi, J. J. Hsieh, and C. M. Wolfe, "Integrated GaAs-AlGaAs double-heterostructure lasers," *Appl. Phys. Lett.*, vol. 27, pp. 241–243, Aug. 1975.
[12] S. Adachi, H. Kawaguchi, K. Takehei, and Y. Noguchi, "InGaAsP/InP buried-heterostructure lasers ($\lambda = 1.5$ μm) with chemically etched mirrors," *J. Appl. Phys.*, vol. 52, pp. 5843–5845, 1981.
[13] E. Garmire, G. Evans, and J. Niesen, "Longitudinal-mode control in GaAs lasers using a three-mirror active-passive cavity," in *Tech. Dig. CLEO'81*, paper FA5.
[14] K. Kishino, Y. Suematsu, K. Utaka, and H. Kawanishi, "Monolithic integration of laser and amplifier/detector by twin-guide structure," *Japan. J. Appl. Phys.*, vol. 17, pp. 589–590, Mar. 1978.
[15] F. K. Reinhart, "Prospects of monolithic integration," in *Proc. of the Soc. of Photooptical Inst. Eng.*, Los Angeles, CA, Feb. 1981, vol. 272, pp. 66–75.
[16] L. A. Coldren, K. Furuya, B. I. Miller, and J. A. Rentschler, "On the formation of planar etched facets in GaInAsP/InP DH for integrated optics," *J. Electrochem. Soc.*
[17] D. Botez, private communication.
[18] P. D. Wright, private communication.
[19] K. L. Conway, A. G. Dentai, and J. C. Campbell, "Etch rates for
[20] two material selective etches on the InGaAsP/InP system," *J. Appl. Phys.*, vol. 53, Mar. 1982.
[20] L. A. Coldren, K. Furuya, B. I. Miller, and J. A. Rentschler, "Combined dry and wet etching techniques to form planar (011) facets in GaInAsP/InP DH," *Electron. Lett.*, vol. 18, pp. 235–237, Mar. 1982.
[21] M. Nakamura and S. Tsuji, "Single-mode semiconductor injection lasers for optical fiber communications," *IEEE J. Quantum Electron.*, vol. QE-17, pp. 994–1005, Apr. 1981.
[22] R. J. Nelson, P. D. Wright, P. A. Barnes, R. L. Brown, T. Cella, and R. G. Sobers, "High-output power InGaAsP ($\lambda = \mu$m) stripe-buried heterostructure lasers," *Appl. Phys. Lett.*, vol. 36, pp. 358–360, 1980.
[23] E. Oomura, T. Murotani, H. Higuchi, H. Namizaki, and W. Susaki, "Low threshold InGaAsP/InP buried crescent laser with double current confinement structure," *IEEE J. Quantum Electron.*, vol. QE-17, pp. 646–650, 1981.
[24] N. Tamari and H. Shtrikman, "High-to low-threshold crescent InGaAsP mesa-substrate buried-heterojunction lasers," *Electron. Lett.*, vol. 18, pp. 177–178, Feb. 1982.
[25] D. Botez, "Constricted double-heterostructure AlGaAs diode lasers: Structure and electrooptical characteristics," *IEEE J. Quantum Electron.*, vol. QE-17, pp. 2290–2309, Dec. 1981.
[26] S. Adachi and H. Kawaguchi, "Chemical etching characteristics of (001) InP," *J. Electrochem. Soc.*, vol. 128, pp. 1342–1349, 1981.
[27] L. W. Stulz and L. A. Coldren, "Orientation of (100) InP wafers," unpublished.
[28] C. A. Burrus, T. P. Lee, and A. G. Dentai, "Short-cavity single-mode 1.3 μm InGaAsP lasers with evaporated high-reflectivity mirrors," *Electron. Lett.*, vol. 17, pp. 954–956, Dec. 1981.
[29] W. Streifer, D. R. Scifres, and R. D. Burnham, "Longitudinal mode spectra of diode lasers," in *Proc. Top. Meet. Integrated and Guided Wave Opt.*, Pacific Grove, CA, 1982 (Opt. Soc. Amer.), paper THB-5.
[30] D. Fekete, W. Streifer, D. R. Scifres, and R. D. Burnham, "High-speed laser modulation with integrated optical injection," *Appl. Phys. Lett.*, vol. 37, pp. 925–978, Dec. 1980.
[31] I.H.A. Fattah and S. Wang, "Semiconductor inferometric laser," in *Proc. Top. Meet. Integrated and Guided Wave Opt.*, Pacific Grove, CA, 1982 (Opt. Soc. Amer.), paper WB-4.
[32] M. W. Fleming and A. Mooradian, "Spectral characteristics of external cavity-Controlled semiconductor lasers," *IEEE J. Quantum Electron.*, vol. QE-17, p. 44, Jan. 1981.
[33] R. Lang and K. Kobayashi, "External optical feedback effects on semiconductor injection laser properties," *IEEE J. Quantum Electron.*, vol. QE-16, pp. 347–355, Mar. 1980.
[34] K. R. Preston, K. C. Woollard, and K. H. Cameron, "External cavity controlled single longitudinal mode laser transmitter module," *Electron. Lett.*, vol. 17, pp. 931–933, Nov. 1981.
[35] K. Utaka, K. Kobayashi, T. Koyama, Y. Abe, and Y. Suematsu, "Single-wavelength operation of 1.53 μm GaInAsP/InP buried heterostructure integrated twin-guide laser with distributed Bragg reflector under direct modulation up to 1 GHz," *Electron. Lett.*, vol. 17, p. 368, May 1981.
[36] S. Kobayashi and T. Kimura, "Injection locking in AlGaAs semiconductor laser," *IEEE J. Quantum Electron.*, vol. QE-17, pp. 681–693, May 1981.
[37] D. W. Smith and D. J. Malyon, "Experimental 1.51 μm monomode fibre link containing an injection locked repeater," *Electron. Lett.*, vol. 18, pp. 43–45, Jan. 1982.
[38] R. L. Rosenberg and L. A. Coldren, "Scattering analysis and design of SAW resonator filters," *IEEE Trans. Sonics Ultrason.*, vol. SU-26, pp. 205–230, 1979.
[39] K. Furuya, B. I. Miller, L. A. Coldren, and R. E. Howard, "A novel deposit/spin waveguide interconnection (DSWI)–Technique for semiconductor integrated optics," in *Proc. Top. Meet. Integrated and Guided Wave Opt.*, Pacific Grove, CA, 1982 (Opt. Soc. Amer.), paper PDP-8; also *IEEE J. Quantum Electron.*, this issue, pp. 1783–1789.

Larry A. Coldren (S'67–M'72–SM'77–F'82) was born in Mifflintown, PA, on January 1, 1946. He received the B.A. degree in physics and the B.S. degree in electrical engineering from Bucknell University, Lewisburg, PA, in 1968, and the M.S. and Ph.D. degrees in electrical engineering from Stanford University, Stanford, CA, in 1969 and 1972, respectively.

Upon completion of his work at Bucknell University, he joined the technical staff of Bell Laboratories, Holmdel, NJ. From 1968 to 1972 he worked in the Microwave Laboratory, Stanford University, under the support of Bell Laboratories. During the 1970's he worked on various ultrasonic device projects at Bell Laboratories. Notable among these were clad fiber long delay lines, ZnO/Si signal processing devices, and coupled SAW resonator filters. In 1979, he shared the SU Transactions Best Paper Award for an article on resonator scattering theory and design. Recently, he has worked in the area of III–V semiconductor integrated optics, using new fabrication techniques, such as reactive ion etching, to create improved structures. He served on the program committee of the IEEE Ultrasonics Symposium from 1975 to 1980, and was elected to the SU Group Ad Com in 1981.

Dr. Coldren is a member of Phi Beta Kappa, Tau Beta Pi, Pi Mu Epsilon, and Sigma Pi Sigma.

Kazuhito Furuya (M'81) was born in Yamanashi Prefecture, Japan, on February 10, 1948. He received the B.S., M.S., and Ph.D. degrees from Tokyo Institute of Technology, Tokyo, Japan, in 1970, 1972, and 1975 respectively.

In 1975 he was a Research Associate and in 1978 he was a Associate Professor at Tokyo Institute of Technology where he worked on microbending losses and mode analysis of optical fibers, and transverse carrier diffusion effects and spontaneous emission factors of semiconductor lasers. From 1980 to 1982 he was a Consultant at Bell Laboratories, Holmdel, NJ, where he worked on applications of chemical etching of GaInAsP/InP for semiconductor integrated optics. He is currently an Associate Professor in the Department of Physical Electronics, Tokyo Institute of Technology, working on a quaternary crystal growth, integrated optics, and optical fibers.

Dr. Furuya is a member of the Institute of Electronics and Communication Engineers of Japan and the Japan Society of Applied Physics.

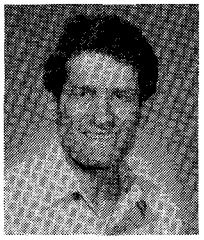

Barry I. Miller was born in Chicago, IL, on October 4, 1937. He received the B.S., M.S., and Ph.D. degrees from the University of Chicago, Chicago, IL, in 1959, 1960, and 1966, respectively.

In 1966 he joined Bell Laboratories, Holmdel, NJ, where he has been engaged in research on superconductors, LPE growth of DH GaAs/AlGaAs lasers, MBE growth of GaInAs/InP lasers, and most recently, LPE growth and etching studies of the GaInAsP/InP system for low threshold single-mode lasers and integrated optics.

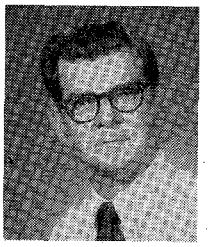

John A. Rentschler was born in Kearny, NJ, on January 19, 1934. After completing an enlistment in the U.S. Marine Corps., he attended RCA Institutes.

In 1960 he joined Bell Laboratories, Holmdel, NJ. During the early 1960's he worked on the "Telstar" project. Later, he worked on both silicon and germanium epitaxy and tantalum thin film projects. In 1972, he joined the research area at Bell Laboratories, where he was active in SAW resonator device research. Recently, he has been working with III-V semiconductors for integrated optics.

Buried Convex Waveguide Structure (GaAl)As Injection Lasers

KATSUHITO SHIMA, KIYOSHI HANAMITSU, AND MASAHITO TAKUSAGAWA

Abstract—**The fabrication technique, analysis of the waveguide property, and lasing characteristics of buried convex waveguide structure (BCS) lasers are described. An improved BCS laser structure having a truncated convex active region was produced by using a novel selective etching technique. It was found that the truncated convex waveguide is very effective in suppressing higher order mode lasing when compared with a convex waveguide. The improved BCS lasers showed stable fundamental transverse mode lasing up to 20 mW/facet, typical threshold current of 20 mA, and an external differential quantum efficiency of 28 percent/facet.**

I. INTRODUCTION

IN the application of injection lasers, linearity of light output-current (I-L) characteristics and stable fundamental transverse mode lasing are the important characteristics of the lasers. It has become evident in the past few years that laser structures having built-in optical waveguide along the junction plane provide stable transverse mode lasing and the linear I-L characteristics. Various kinds of lasers having built-in refractive index distribution along the junction plane have been devised and have been demonstrated to provide stable transverse mode lasing, among which transverse junction lasers [1], rib waveguide lasers [2], buried heterostructure (BH) lasers [3], [4], and channeled substrate buried heterostructure (CSB) lasers [5], [6], are notable examples.

The CSB laser is unique in that it has a convex active region embedded in a lower refractive index material, and built-in refractive index along the junction plane is achieved by the thickness variation of the active region [6]. CSB lasers were first reported by Burnham *et al.* [5] and Kirkby *et al.* [6], and were later modified to improve lasing characteristics [7], [8]. However, it is supposed that CSB lasers do not consistently realize fundamental transverse mode lasing.

Recently, we reported a new type of CSB laser [9], called a buried convex waveguide structure (BCS) laser, which has a narrow active region (3.0-3.5 μm) and consistently realizes fundamental transverse mode lasing. However, fundamental mode lasing was limited below the output power of 5-6 mW/facet. This may be why the width of the active region is wider than the cutoff width for higher order mode lasing, even in a BCS laser. One possibility for achieving fundamental mode lasing at a higher power level is to make the width of the active region narrower than the cutoff width, but it is difficult to realize such a narrow active region using a GaAs substrate [5], [10]. Another possibility is to realize a waveguide in which there is a large difference in the scattering loss between the fundamental mode and higher order modes to suppress higher order mode lasing [11].

In this paper, we report an improved BCS laser having a truncated convex active region. Its fabrication procedures using a novel selective etching technique and the waveguide analysis are described. In the truncated convex waveguide, the fundamental mode mainly distributes in the center flat region with small loss, but the higher order modes distribute over the tapered region causing large scattering loss. Owing to such waveguide properties, we obtained stable fundamental transverse mode lasing up to 20 mW/facet, a typical threshold current of 20 mA, and an external differential quantum efficiency of 28 percent/facet. It was also found that the out-

Manuscript received March 2, 1982.
The authors are with Fujitsu Laboratories, Ltd., Kawasaki, Japan.

0018-9480/82/1000-1676$00.75